Journal of Aerospace Information Systems, Volume 20, Issue 11, November 2023, pp. 690-701
DOI:10.2514/1.I011256

Data-driven Diagnosis of Multicopter Thrust Fault Using Supervised Learning with IMU Sensor

Taegyun Kim * and Seungkeun Kim †
Chungnam National University, Daejeon, KS015, South Korea

Hyo-Sang Shin ‡
Cranfield University, Cranfield, MK43, United Kingdom

This study proposes a data-driven fault diagnosis for multicopter UAVs that uses the principal direction vector of IMU sensor signals calculated by principal component analysis (PCA). The main idea comes from the fact that a normal sphere-shaped distribution of the sensor data changes to a specific elliptical shape under a certain thrust fault situation. The fault diagnosis is based on classification and regression using supervised learning with the gyroscope and accelerometer datasets of an IMU. We analyze the performance of the proposed approach depending on different learning algorithms. To verify the diagnostic performance, ground experiments with a hexacopter on the gimbaled jig are performed for various cases of damaged propellers. Then, the applicability of the proposed data-driven fault diagnosis is confirmed by analyzing the accuracy of the fault's location and degree.

Nomenclature

ϕ, θ, ψ	=	Roll, pitch, and yaw angles
I_{xx}, I_{yy}, I_{zz}	=	Moment of the inertia of the UAV
F_x, F_y, F_z	=	Components of force vector
L, M, N	=	Moments acting on the center of gravity
$\tau_{\phi_{gyro}}, \tau_{\theta_{gyro}}$	=	The gyroscopic forces of each axis
J_A	=	Actuator inertia
Ω_k	=	Rotation speed of the k-th actuator
f_k	=	Produced thrust by the k-th actuator
c_T	=	Thrust coefficient
d	=	Length of the hexacopter UAV arm
c_Q	=	Counter-torque coefficient

*Graduate student, Department of Aerospace Engineering, ktg92@o.cnu.ac.kr.
†Professor, Department of Aerospace Engineering, skim78@cnu.ac.kr, Senior Member
‡Professor, School of Aerospace Transport and Manufacturing, h.shin@cranfield.ac.uk, Senior Member

a_x, a_y, a_z = Acceleration values measured by accelerometers

g_x, g_y, g_z = Gyroscope data

X = Data matrix

U = Left singular vectors of X

Σ = Singular values of X

W = Right singular vectors of X

I. Introduction

A multicopter unmanned aerial vehicle (UAV) can perform vertical takeoff and landing (VTOL) and hover flight operations. Multicopter UAVs with more than four actuators have the advantages of actuator redundancy and fault tolerance when compared to traditional aircraft such as helicopters [1]. However, multicopter UAVs have the disadvantage of having difficulty performing stable flight missions if a problem occurs with the actuator during flight. Because the multicopter UAV attains flight using only the thrust of its actuators, the thrust fault is directly linked to the overall multicopter UAV safety. In addition, actuators are susceptible to crash and damage and thus have a possibility of faulting the entire UAV system. When an actuator is damaged due to a fault during flight, human fatality, and property damage can occur owing to collisions and falls [2]. The multicopter UAV may experience poor tracking performance or excessive vibrations if some actuators fault.

Safety is the most critical concern in UAV operations. Unfortunately, small UAVs cannot conduct fault diagnosis autonomously using their onboard sensors due to hardware limitations. Because it is difficult to mount additional sensors for fault diagnosis and check for faults in a small multicopter UAV, there are frequent cases of flying without knowing the fault that occurred in the actuator in advance [3]. According to the Survey report on the unmanned vehicle industry in Korea [4], it was investigated that there were many faults in the actuator parts, such as propellers, motors, and motor arms. Figure 1 displays the investigation results of parts that faulted more than five times during one year of operation, focusing on companies that operate UAVs in Korea. The numbers indicate the frequency of occurrence, and the investigation found that many component faults occurred on the propeller and frame motor side.

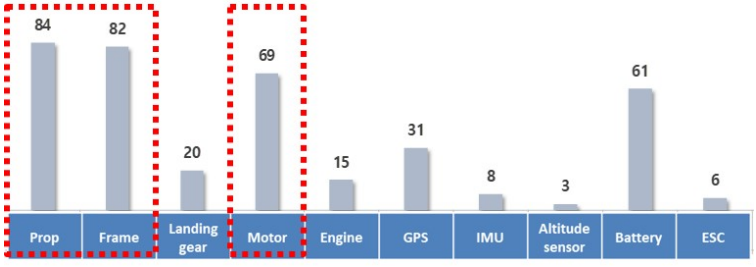

Fig. 1 The number of UAV's fault depending on the equipment.[4]

The reliance on human efforts such as visual inspection for preflight checks increases the operational cost and limits. Therefore, it is essential to diagnose the fault of the actuator of the UAV during the preflight phase without additional sensors.

A. Related work

Given the increasing interest and expected widespread use of UAVs, accurate fault detection and diagnosis (FDD) methods are critical for ensuring the safety and reliability of UAVs. In addition, since the performance of fault tolerance control is determined according to the FDD method result [5][6], a study on a high-accuracy FDD method is being actively conducted. FDD methods can be divided into two main categories, which have been proposed based on model-based methods such as Kalman filter and dynamics models [7][8] and data-driven methods.

The model-based FDD method identifies the fault mechanism and then uses the associated fault physical model to determine normal or abnormal conditions [9][10]. Faults can be diagnosed with high accuracy if the target model is known precisely. However, it is difficult to obtain an actual physical failure model, and if the model accuracy is low, the diagnostic accuracy also decreases [11]. Pin lyu *et. al.* [12] presented a fault diagnosis method for sensors in the vertical direction of a multicopter UAV capable of dealing with the z-axis accelerometer, and Ron wang *et. al.* [13] presented the same concept using a barometer sensor.

In the data-driven FDD method, when collecting data indicating the health of an object, a different fault diagnosis method is used depending on whether the state information of the object is known or not. Suppose the state information on whether the target is normal or abnormal is unknown. In that case, fault diagnosis is generally performed by unsupervised learning, or semi-supervised learning [14]. On the other hand, fault diagnosis is performed by classifying supervised learning-based data if the state information is known. The data-driven FDD method has the advantage of diagnosing without knowing the fault physics model of the target. Shin *et. al.* [15] conducted a battery anomaly detection study using the sequence-to-sequence type deep learning Model.

Table 1 Comparison of real-time fault diagnosis types with relevant studies

References	UAV types	Fault types	Methods
Jaramillo,Jesse, *et. al.*, 2022 [16]	Hexacopter	Thrust fault	PWM signal
Ray *et. al.*, 2021 [17]	Qaudcopter	Thrust fault	Skewness scanning
Ghalamchi, *et. al.*, 2019 [18]	Quadcopter, Hexacopter	Propeller fault	Kalman filter
Ochoa, C. A. and Atkins, E.M., 2018 [19]	Quadcopter	Control fault	Gaussian naive bayes learning
Pourpanah, F. *et. al.*, 2018 [20]	Quadcopter	Thrust fault	Fuzzy logic
Xi Chen and He Ren, 2018 [21]	Fixed-wing	System fault	Hierarchical bayesian network

Most studies have focused on the diagnosis and handling of real-time thrust faults during flight. Table 1 summarises the

real-time fault diagnosis studies that compare the UAV used, the different types of fault, and the method implemented. Jaramillo *et. al.* [16] experimentally validated the thrust fault detection and dynamic control allocation for a hexacopter UAV thrust fault by using PWM signals sent to each actuator's Electronic Speed Control (ESC). Ray *et. al.* [17] proposed to detect a thrust fault by using a skewness scanning method. Ghalamchi *et. al.* [18] have presented the propeller fault detector that uses accelerometer data to detect abnormalities in multicopter UAV propellers. Ochoa and Atkins [19] used a traditional supervised learning method for thrust fault diagnosis. Pourpanah [20] also used vibration data and current data to detect the anomalous condition of the UAV. Xi Chen and He Ren [21] performed hierarchical bayesian network-based learning to diagnose fault types and efficiency.

The real-time FDD methods have the advantage of coping with faults when faults occur during flight. However, there is a disadvantage in that it cannot prevent in advance, which causes financial and time losses during the flight mission. In addition, in the case of a hexacopter UAV, even if one actuator is faulted, there is a slight stagger, and the control can be maintained only with PID control. However, it may cause additional faults by straining other actuators. Therefore, it is necessary to study the FDD method during the preflight phase, which involves ground inspection before flight. Table 2 shows the comparison of preflight or postflight diagnosis types with relevant studies.

Table 2 Comparison of preflight or postflight fault diagnosis types with relevant studies

References	UAV types	Fault types	Methods
Mohamad Hazwan Mohd, and Wan Rahiman, 2022 [22]	Quadcopter	Motor arm fault	Neuro-fuzzy, Neural network
Milad Memarzadeh. *et. al.*, 2022 [23]	Fixed-wing	Control fault	Compact clustering via label propagation
Kim, J. *et. al.*, 2021 [24]	Quadcopter	Thrust fault	Gaussian process regression
Zhenyu zhou and Yanchao Liu., 2021 [3]	Quadcopter	Misplaced payload, Propeller fault	Nonlinear least squares model
Iannace. G. *et. al.*, 2019 [25]	Quadcopter	Propeller fault	Neural network
Ghalamchi. B. and Mueller. M., 2018 [26]	Quadcopter	Propeller fault	Spectral analysis
Lee, C. *et al.*, 2018 [27]	Fixed-wing	System fault	Pattern analysis

Mohd and Rahiman [22] measured vibration using a sensor and experimentally validated the motor arm fault detection by using fuzzy, neuro-fuzzy, and neural networks. Milad Memarzadeh. *et. al.* [23] conducted a study on diagnosing multiple control fault problems using compact clustering via label propagation method (CCLP), one of the semi-supervised learning approaches. Kim. J *et al.* [24] conducted a study to diagnose the degree of thrust fault by learning the predicted disturbance value from the disturbance observer using Gaussian process regression in the preflight phase. Zhou and Liu [3] developed a smart landing platform using a nonlinear least-square model that is possible to diagnose where the fault is and whether there is a problem with the payload position. Iannace *et. al.* [25] detected propeller faults by learning the sound pressure level. Ghalamchi and Mueller [26] detected the propeller fault by performing spectral analysis using the Fourier transform. Lee. C *et al.* [27] conducted a fault diagnosis study using pattern analysis by learning the pattern of labeled data using fault record data.

B. Main contribution

In this paper, a part of the propeller was broken to simulate the thrust fault. Although the experiment in this paper was conducted using propeller fault, if the fault of the motor itself occurs completely or partially, it is thought that a similar trend will occur in the cluster data of the accelerometer or gyroscope. In this sense, the results of this study can be easily applied to the thrust fault.

Unlike previous studies, this study used principal component analysis (PCA) of accelerometer and gyroscope signals to diagnose thrust faults during the pre-flight phase of hexacopter UAVs. Subsequently, the PCA of the data is trained for supervised learning to diagnose the thrust fault. The main contributions in this study are summarized as follows.

The first contribution is that the proposed method only uses the data from the IMU sensor installed default for automatic control. Normally, the thrust fault diagnosis uses both an IMU sensor and RPM command or measurement. The existing FDD methods often require separate equipment such as an RPM sensor or a force balance for the fault diagnosis in the pre-flight phase. The proposed approach uses only accelerometer or gyroscope data of the IMU sensor for diagnosis and can identify even the location and degree of the thrust fault.

The second contribution is to establish a standard FDD method that can be used for any hexacopter UAV with the same actuator arrangement. It can be used as good evidence to support the judgment in inspections such as minor thrust faults, basic maintenance, and preventive maintenance, which are difficult to judge only by visual inspection during the current operation of the UAV.

Lastly, we developed a preflight FDD algorithm for diagnosing thrust faults of multicopter UAVs using jig testing on the ground. The proposed FDD method can be used as a basis for preventive maintenance and help with visual inspection tests by presenting a fault diagnosis method that can be used in the preflight phase.

This paper is organized as follows: Section II introduces the hexacopter UAV dynamic model and shows the feature extraction process by the PCA, which describes the supervised learning in detail and what was used. Section III explains the experimental setup and training procedure used to obtain the training data. In Section IV, the performance of the proposed fault diagnosis method according to the dataset and supervised learning algorithms was compared. Section V offers conclusions of the paper with pointers for future work.

II. Background

A. Hexacopter UAV Dynamic Model

A configuration of the hexacopter UAV is shown in Figure 2, which is considered as a 6-Degree of Freedom. x_B, y_B, z_B axes are originate at the mass center of the hexacopter UAV. The equations of the motion of the hexacopter UAV dynamics obtained from Newton's laws are as follows [28] :

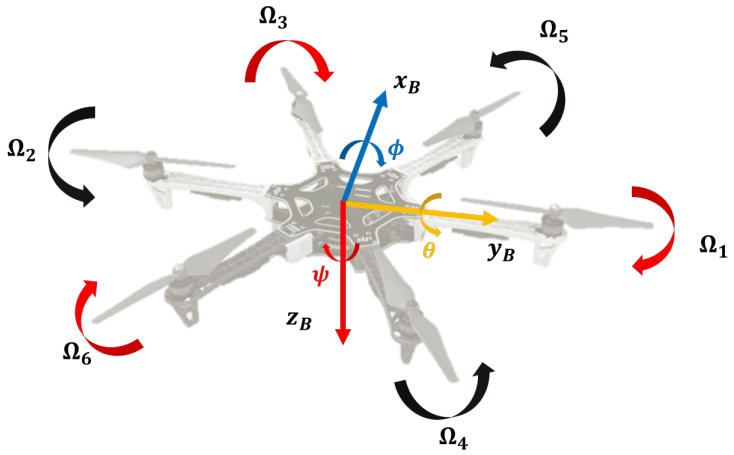

Fig. 2 The hexacopter UAV with PNPNPN configuration. P is a rotor rotates clockwise, and N is counter-clockwise.

$$
\begin{cases}
\dot{u} = rv - qw - gsin\theta + F_x/m \\
\dot{v} = -ru - pw - gsin\phi cos\theta + F_y/m \\
\dot{w} = qu - pv - gcos\phi cos\theta + F_z/m \\
\dot{p} = (I_{yy} - I_{zz})qr/I_{xx} + \tau_{\phi_{gyro}}/I_{xx} + L/I_{xx} \\
\dot{q} = (I_{zz} - I_{xx})pr/I_{yy} + \tau_{\theta_{gyro}}/I_{yy} + M/I_{yy} \\
\dot{r} = (I_{xx} - I_{yy})pq/I_{zz} + N/I_{zz}
\end{cases} \tag{1}
$$

where u, v, and w are the longitudinal, lateral, and vertical body velocities, and p, q, and r are the roll, pitch, and yaw rates, respectively. The rates can be measured using gyroscopes. g is the acceleration of gravity, and ϕ, θ, and ψ are the Roll, Pitch, and Yaw. I_{xx}, I_{yy}, I_{zz} are the moments of the inertia of the UAV, respectively. In equation 1, F_x, F_y, F_z are components of the force vector and L, M, N are moments acting on the center of gravity.

$\tau_{\phi_{gyro}}, \tau_{\theta_{gyro}}$ represent the gyroscopic forces of each axis. $\tau_{\phi_{gyro}}, \tau_{\theta_{gyro}}$ are as follows:.

$$
\begin{cases}
\tau_{\phi_{gyro}} = -J_A q(\Omega_1 - \Omega_2 + \Omega_3 - \Omega_4 + \Omega_5 - \Omega_6) \\
\tau_{\theta_{gyro}} = J_A p(\Omega_1 - \Omega_2 + \Omega_3 - \Omega_4 + \Omega_5 - \Omega_6)
\end{cases} \tag{2}
$$

where J_A is the actuator inertia. $\Omega_k, k = 1, 2, 3, 4, 5, 6$ represents the rotation speed of the i-th actuator. Given the hexacopter UAV dynamic model shown in Figure 2, the variables are calculated by [29]:

$$\begin{cases} L = c_T d(-\Omega_1^2 + \Omega_2^2) - c_T \frac{d}{2}(\Omega_3^2 - \Omega_4^2 - \Omega_5^2 + \Omega_6^2) \\ M = c_T \frac{\sqrt{3}}{2} d(\Omega_3^2 - \Omega_4^2 + \Omega_5^2 - \Omega_6^2) \\ N = c_Q(\Omega_1^2 - \Omega_2^2 + \Omega_3^2 - \Omega_4^2 + \Omega_5^2 - \Omega_6^2) \end{cases} \tag{3}$$

where $f_k = c_T \Omega_k^2, k = 1, 2, 3, 4, 5, 6$ is the produced thrust by the i-th actuator, c_T is the thrust coefficient, and d represents the length of the hexacopter UAV arm. c_Q is the counter-torque coefficient.

Acceleration values measured by accelerometers (a_x, a_y, a_z) include several types of acceleration, such as gravitational acceleration, and acceleration that occurs when the velocity or direction of the UAV changes. The accelerometer values were as follows:

$$\begin{bmatrix} a_x \\ a_y \\ a_z \end{bmatrix} = \begin{bmatrix} \dot{u} \\ \dot{v} \\ \dot{w} \end{bmatrix} + \begin{bmatrix} 0 & w & -v \\ -w & 0 & u \\ v & -u & 0 \end{bmatrix} \begin{bmatrix} p \\ q \\ r \end{bmatrix} + g \begin{bmatrix} sin\theta \\ -cos\theta sin\phi \\ -cos\theta cos\phi \end{bmatrix} \tag{4}$$

B. Feature Extraction by PCA

PCA is the process of computing the principal components and is used to find a change of basis on the data [30]. The PCA is defined as an orthogonal linear transformation. Suppose X is an $n \times p$ data matrix,

$$X = \begin{bmatrix} x_{11} & x_{12} & \cdots & x_{1p} \\ x_{21} & x_{22} & \cdots & x_{2p} \\ \vdots & \vdots & \vdots & \vdots \\ x_{n1} & x_{n2} & \cdots & x_{np} \end{bmatrix} \tag{5}$$

where n represents the number of data samples, each column provides a particular feature.

The principal components are computed using singular value decomposition (SVD) of the data matrix [31]. The SVD of X is expressed as follows:

$$X = U \Sigma W^T \tag{6}$$

where Σ is a rectangular diagonal matrix of positive numbers σ_k, called the singular values of X; U is orthogonal unit

vectors of length n called the left singular vector of X; W is an orthogonal unit vector of length p and called the right singular vectors of X. In this case, the right singular vector is the same as the principal direction vector of the dataset. The matrix $X^T X$ can be written as:

$$\begin{aligned} X^T X &= W\Sigma^T U^T U\Sigma W^T \\ &= W\Sigma^T \Sigma W^T \\ &= W\Sigma^2 W^T \end{aligned} \tag{7}$$

A comparison with the eigenvector of $X^T X$ establishes that W is equivalent to the eigenvectors of $X^T X$.

This section examines the acquisition of the training data and extraction of the features needed to develop the fault diagnostic method. Using Equations 5 and 6, $X_{acc}, X_{gyro} \in R^{n\times 3}$ composed of $X-$,$Y-$, and $Z-$axis accelerometer data (a_x, a_y, a_z) and gyroscope data (g_x, g_y, g_z) can be expressed as follows:

$$X_{acc} = U_a \Sigma_a W_a^T = \begin{bmatrix} a_{x,1} & a_{y,1} & a_{z,1} \\ a_{x,2} & a_{y,2} & a_{z,2} \\ \vdots & \vdots & \vdots \\ a_{x,n} & a_{y,n} & a_{z,n} \end{bmatrix} \tag{8}$$

$$X_{gyro} = U_g \Sigma_g W_g^T = \begin{bmatrix} g_{x,1} & g_{y,1} & g_{z,1} \\ g_{x,2} & g_{y,2} & g_{z,2} \\ \vdots & \vdots & \vdots \\ g_{x,n} & g_{y,n} & g_{z,n} \end{bmatrix} \tag{9}$$

where X_{acc} is the accelerometer matrix, and X_{gyro} is the gyroscope matrix. U is composed of $n \times n$ left singular vectors, Σ is the singular value matrix, and W_a^T is a 3×3 matrix comprised of nine feature values with rotation components. In addition, W_g^T represents a rotation of the group coordinate axes of the IMU sensor data. The principal component rotation value of the accelerometer, W_a^T, and gyroscope data, W_g^T, was used as the feature data for supervised machine learning-based fault diagnosis.

In Figure 3, the black sphere is a collection of accelerometer data at the time of the preflight test if the multicopter is healthy. If the actuator is normal, accelerometer data are distributed on a sphere even if the vibration occurs. Depending on the measured data, the shape of the sphere is maintained, and only the size changes. When the thrust fault occurs, the

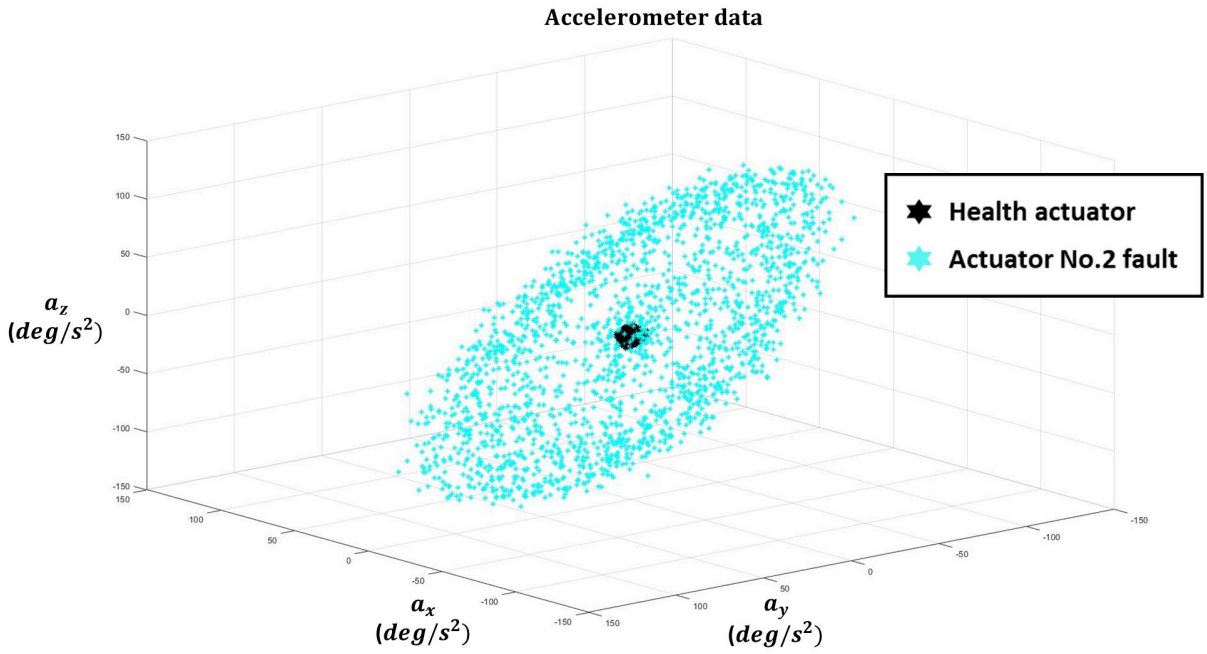

Fig. 3 Scatter plot of the accelerometer in a 3-D feature space.

specific-axis accelerometer values get more significant due to vibration. This vibration makes the accelerometer dataset to be a particular ellipsoidal shape. The cyan ellipsoidal shape shows the single thrust fault case.

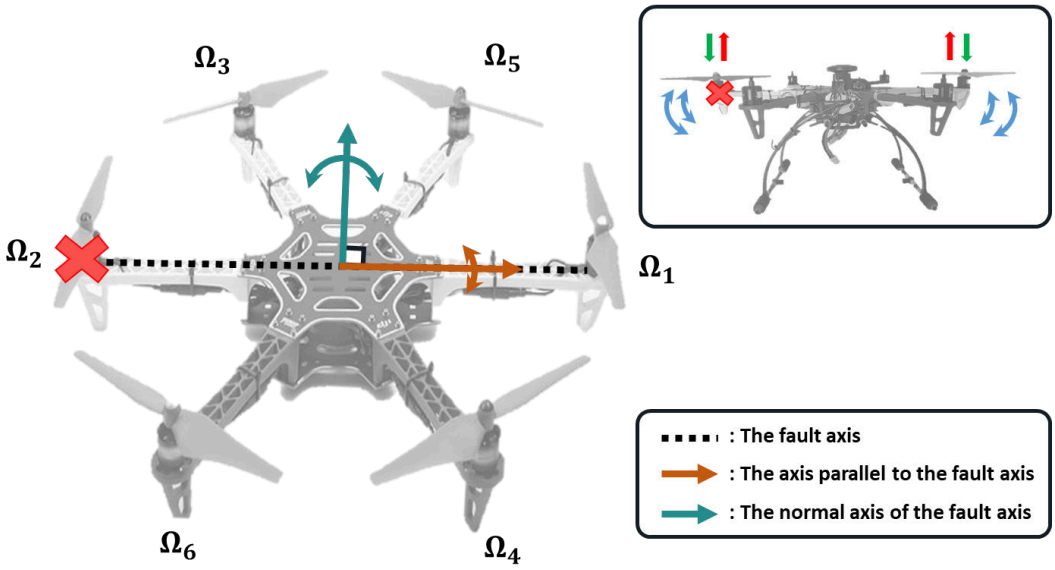

Fig. 4 The movement of the multicopter UAV in the case of the actuator no.2 fault

Figure 4 illustrates the movement of the multicopter UAV in the case of the actuator number 2 fault. When a single thrust faults and the hexacopter begins to lose its horizontal attitude, the attitude controller levels the attitude by increasing the power in the actuator opposite to the faulty actuator to maintain horizontal attitudes.

As a result, the up-and-down vibration of the actuator on the fault axis causes rotation about an axis parallel to and normal axis to the fault axis. This movement creates a principal vector of specific accelerometers and gyroscopes data sets for each fault case. According to Equation 4, it is possible to obtain accelerometer data that form a specific elliptical shape in each case.

C. Thrust fault Diagnosis Model

For learning the fault diagnosis model, detailed knowledge of the internal dynamics of the system is not necessary. Instead, the training data is the source of information about the behavior of the system. Supervised machine learning requires labeling previously occurring fault cases in the training data and is typically utilized for data-driven cause inference. A fault diagnosis model is developed using artificial neural networks (ANN) [32] and support vector machines (SVM) [33].

This study develops a novel fault diagnosis model against the thrust faults of UAVs to address safety concerns. We propose the following steps to diagnose the fault.

Step 1: Ground test for preflight examination or possibly flight test for postflight examination

Step 2: Acquisition of accelerometer and gyroscope dataset

Step 3: Extraction of singular values and vectors

Step 4: Training with the supervised learning

Step 5: Diagnosis of the faulty actuator

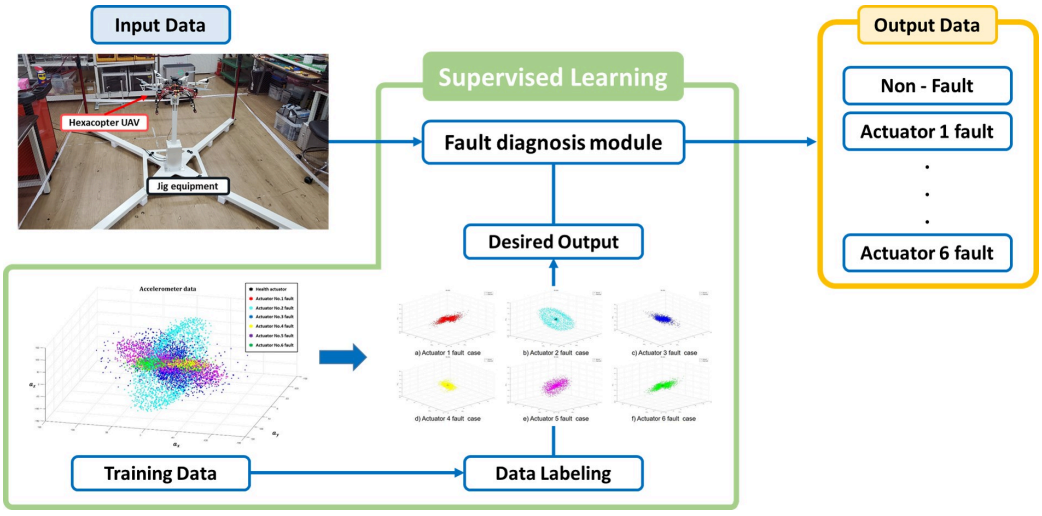

Fig. 5 A flow diagram of the fault diagnosis method

III. FAULT DIAGNOSIS MODEL

A. Experimental Setup

1. Thrust fault Injection

The proposed fault diagnosis system detects which specific actuator is faulty. The principal case considered in this study concerns the damage to one of the actuators in the proximity of the propeller tip. This specific case was chosen because the extremities of the actuators are more susceptible to damage during regular UAV flight mission operations and therefore a frequent fault case. Figure 6 shows the shape of the damaged actuator considered in the experiment.

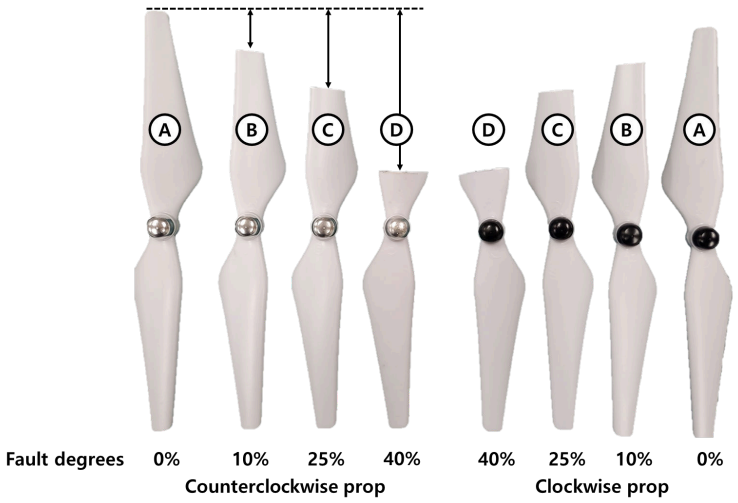

Fig. 6 The shape of the damaged actuator

In Figure 6, A is a normal propeller, B is 10 %, C is 25 %, and D is a propeller simulating a damaged situation of 40 % of the total length. After acquiring the IMU data for the four cases, supervised learning is performed to diagnose the location and degree of the fault.

2. Hardware Setup

The IMU sensor data was collected using a PIXHAWK, which has a high-rate data logger capable of recording onboard sensor signals with a sampling rate of 500 Hz. The axes of the IMU sensor are set as follows:

- The x-axis positive direction is heading to the front.
- The y-axis positive direction is to the right.
- The z-axis is positive downwards.

Table 3 and Figure 7 show the physical parameters and the actuator number of the hexacopter UAV used in the experiments, respectively. The red dotted line in Figure 7 represents the damaged actuator.

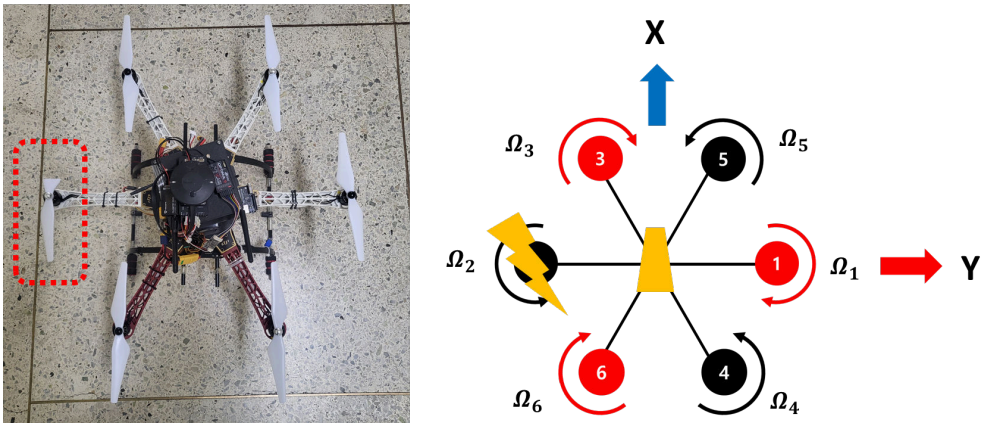

Fig. 7 The actuator locations of the hexacopter UAV

Table 3 Physical paramters of the hexacopter UAV

Physical parameters	Specification
Total mass m	1.78 kg
Arm length d	0.28 m
I_{xx}, I_{yy}	9.06× 10^{-3} kg·m^2
I_{zz}	11.65× 10^{-3} kg·m^2

3. Fault data Acquisition

Figure 8 shows the thrust fault diagnosis system using the jig equipment. The jig test equipment was used to get the training data needed to create the thrust fault diagnostic model and perform the preflight diagnosis. This data is supplied to the fault diagnostic method to assess the degree of fault of the UAV and to determine whether the flight is possible.

Fig. 8 The actuator FDD method test using the jig equipment

Our proposed FDD method is based on supervised learning of which each data point of the hexacopter UAV thrust fault is labeled. Accelerometer and gyroscope training data was acquired from the damaged propeller (shown in Figure 6) when the hexacopter was operated for 10 s. The ground jig equipment with a real hexacopter UAV was then used to verify the performance of the proposed system, as shown in Figure 8. The 3-DOF gimbal, mounted on a ground jig equipment, allows the hexacopter UAV to control its attitude for the ground test. The hexacopter UAV was developed based on a DJI's F550 frame.

4. Training the Feature dataset from IMU signals

Flight data during various thrust fault situations is required to develop an actuator FDD method through supervised machine learning methods. In this study, training data was acquired by preflight test a multicopter on ground jig equipment during a specific thrust fault condition. Figure 9 shows the measured accelerometer datasets.

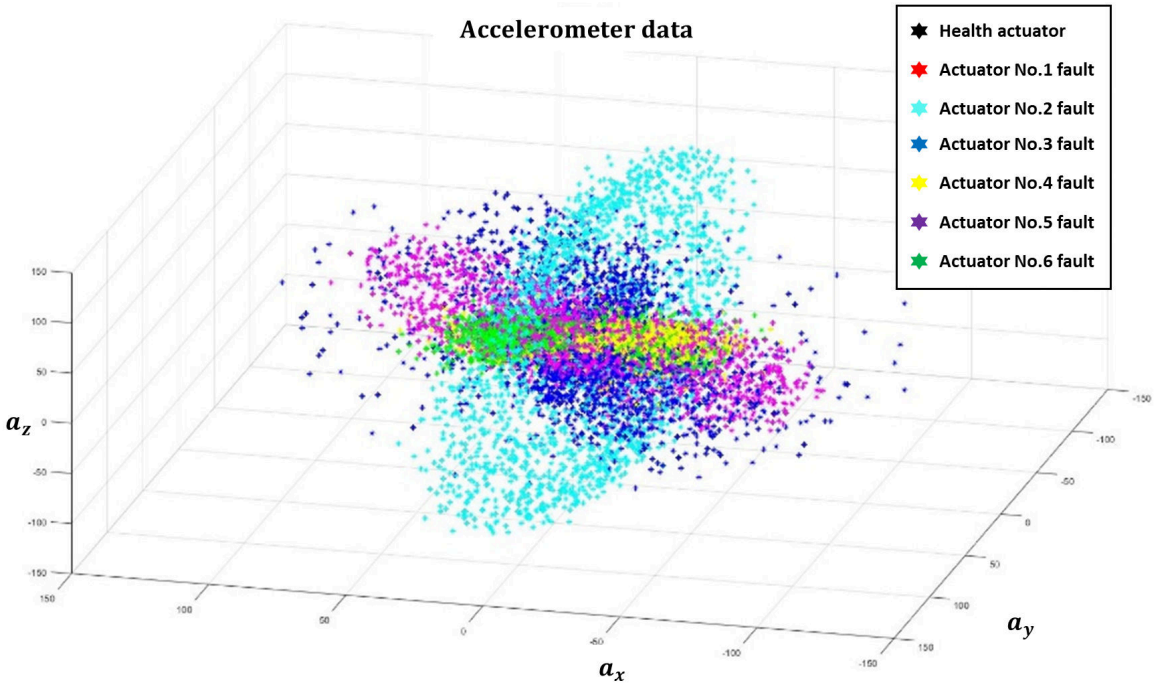

Fig. 9 Scatter plot of accelerometer data in a 3-D feature space

Comparisons were made between the performance of the ANN and SVM algorithms that were trained using accelerometers and gyroscope sensor signal populations. Figure 10 shows a flow diagram of the proposed procedure. The input features, that is the result of the accelerometer and gyroscope data's PCA, distinguish between normal and defective actuator cases. The trained output shows the classification of the extracted features from the acquired and preprocessed signals in the diagnosis of the thrust fault.

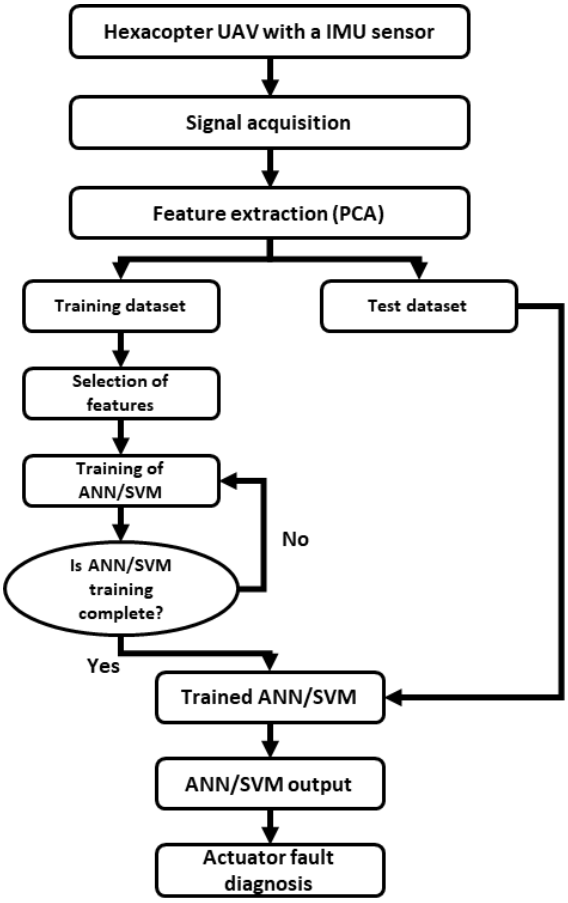

Fig. 10 A flow diagram of the FDD method procedure

IV. FAULT DIAGNOSIS RESULT

This section analyzes the results of the proposed fault diagnosis method. The proposed method was implemented using MATLAB 2021a software. A total of 500 sample data points were used for the performance evaluation. Figure 11 provides a detailed discussion on the performance evaluation metrics.

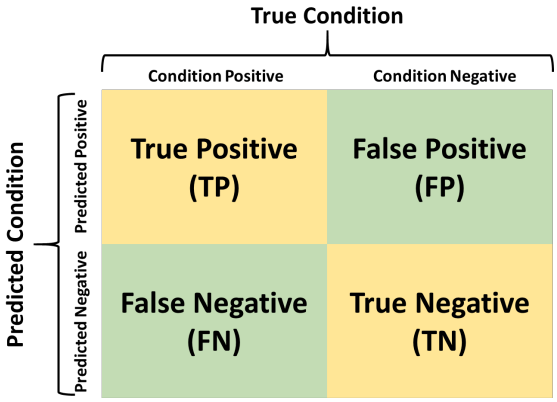

Fig. 11 Confusion Matrix

Where a "True Positive (TP)" means that the system predicts a faulty actuator as faulty. A "True Negative (TN)" is that the system predicts a non-faulty actuator as non-faulty. "False Positive (FP)" means that the system predicts non-faulty actuator as faulty. Lastly, "False Negative (FN) implies that as a faulty actuator is declared as non-faulty.

First, the performance of the proposed FDD method was calculated based on the accuracy, prediction speed, and training times. "Accuracy" is calculated as the ratio of correctly predicted observations to the total number of observations. The accuracy of the method should be as high as possible. The accuracy is defined by the following equation:

$$Accuracy(\%) = \frac{TP + TN}{TP + TN + FP + FN} \times 100 \tag{10}$$

"Prediction speed" refers to the number of times the module predicts data per second. The higher this value, the more data can be diagnosed in the same amount of time. "Training time" refers to the time it takes to learn the diagnostic module. In other words, the shorter the training time, the faster the module is learned. The diagnostic results of the ANN and SVM algorithms are compared and summarized in Table 4. When comparing percentage accuracy and learning time, the ANN using accelerometers provides better accuracy and faster learning time than the others. Although the prediction speed was the second level in these cases, ANN is suitable for use. Therefore, this study adopted the ANN using accelerometers for thrust fault diagnosis.

Table 4 Performance values of different type diagnosis method

Algorithm type	Accuracy	Prediction speed	Training times
SVM (Accel)	95.6 %	2,300 obs/sec	1.4393 sec
ANN (Accel)	**99.3 %**	5,500 obs/sec	**1.1029 sec**
SVM (Gyro)	94.8 %	2,200 obs/sec	1.7237 sec
ANN (Gyro)	98.1 %	**6,000 obs/sec**	1.3835 sec

A. Performance Parameter

The performance of the proposed fault diagnosis method was measured based on True Positive Rate (TPR), False Negative Rate (FNR), Positive Predictive Value (PPV), and False Discovery Rate (FDR). These parameters have been used to judge the performance of the FDD method [34],[35]. The TPR is used to measure the percentage of actual positive candidates. When performing multiple comparisons, the FNR is the probability of falsely rejecting the null hypothesis for a particular test. The system with a higher TPR and lower FNR claims had higher efficacy. The PPV measures the probability of a false region being predicted as a false region. The FDR provides information about how many true regions have been detected as false regions among the overall detected cases.

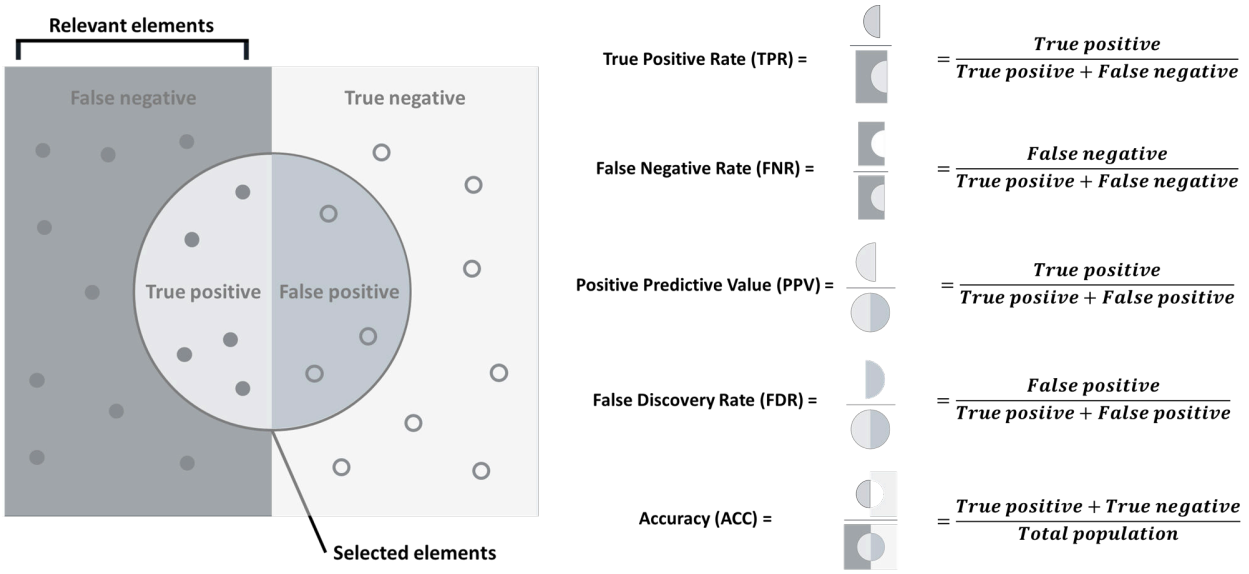

Fig. 12 Performance parameters

B. Fault diagnosis performance (detect location)

Supervised learning uses the right singular vector of the accelerometer data population obtained through the PCA. The thrust fault diagnostic model was created using an ANN algorithm. Figure 13 shows a scatter plot of the trained principle components. Each scatter in the figure represents the results of dimensionality reduction of the data to be diagnosed. The values of the main axis calculated through the PCA are represented by the x-axis and y-axis labels. This shows a certain trend for each thrust fault. Each scatter point represent the PCA value of the cluster data and are well classified to distinguish the faulty actuator number. By analyzing the scatter result in Figure 13, the group data formed for each fault case becomes distinct. In this experiment, even if a single case in actuator 1 is misdiagnosed as the fault in actuator 6, everycase else is correctly diagnosed with a high accuracy.

Figure 14-15 show the confusion matrix plot to understand how the selected classifier performs in each class. The rows show the true class and the columns represent the predicted class. The diagonal cells show the true class and the predicted class match. If these diagonal cells are of high percentage, the classifier correctly classifies the observations of this true class.

The result shown in Figure 14 provides an analysis of the predictions made on the test data using the TPR and FNR, and Figure 15 shows the PPV and FDR. The TPR and PPV are shown in blue for the correctly predicted cases in each class, and the FNR and FDR are shown in red for the incorrectly predicted cases in each class. Table 5 presents the diagnosis of 140 data based on the TPR, FNR, PPV, and FDR, calculated using the confusion matrix.

The 100 % of TPR was accomplished for thrust fault number 1, 2, 3, 4, 5, and healthy class and 95 % for number 6 class, respectively. At the same time, the FDD method attained the FNR value of 0 % and 5 %, respectively, for these classes.

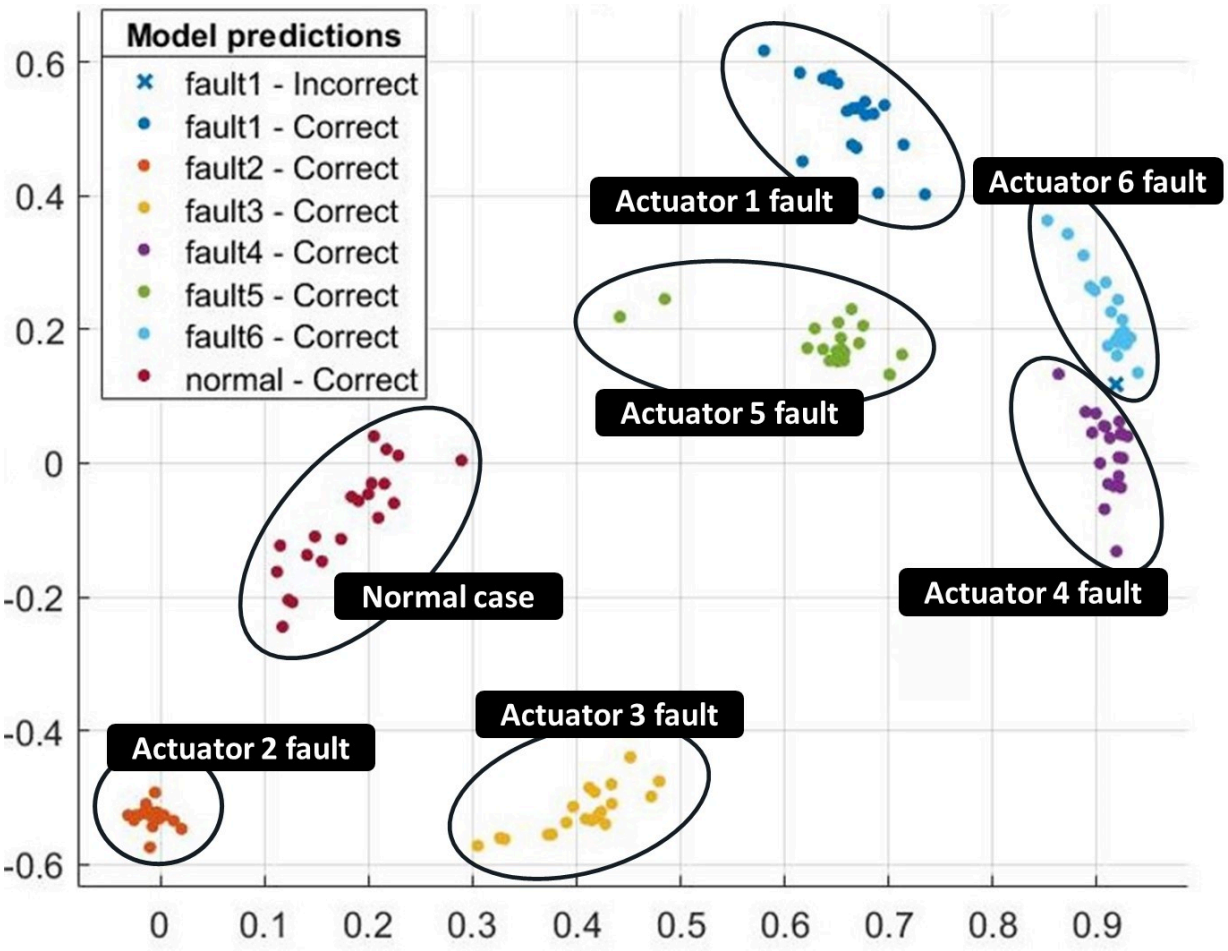

Fig. 13 The scatter plot of the trained principle components

The proposed method obtained the PPV 100 % for the number 2, 3, 4, 5, 6, and healthy class and 95.2 % for the number 1, respectively. Whereas the FDR values were determined as 0 % for number 2, 3, 4, 5, 6, and healthy class, 4.8 % for the number 1 class. The FNR result shows about 4.8 % of cases in which the number 1 actuator is diagnosed to be faulty when the number 1 actuator is not a fault. Also, the FDR results mean that about 5 % of cases are diagnosed as non-faulty in the number 6 actuator when the number 6 actuator is faulty. In other cases, it is confirmed that the proposed diagnosis method can be used for diagnosis with 100 % accuracy.

C. Fault diagnosis performance (degree of damages)

ANN-based regression is performed using the right singular vector data of the accelerometer obtained through PCA to learn the degree of actuator damage. Figure 16 displays the results of the degree of damages-value regression learning. Figure 15a represents that a comparison graph shows little error between the true value and the prediction. As a result, it was calculated close to linear. Figure 15b means the errors between the prediction and true for each thrust fault. Regression learning results that are close to a linear function are generated depending on the degree of the thrust

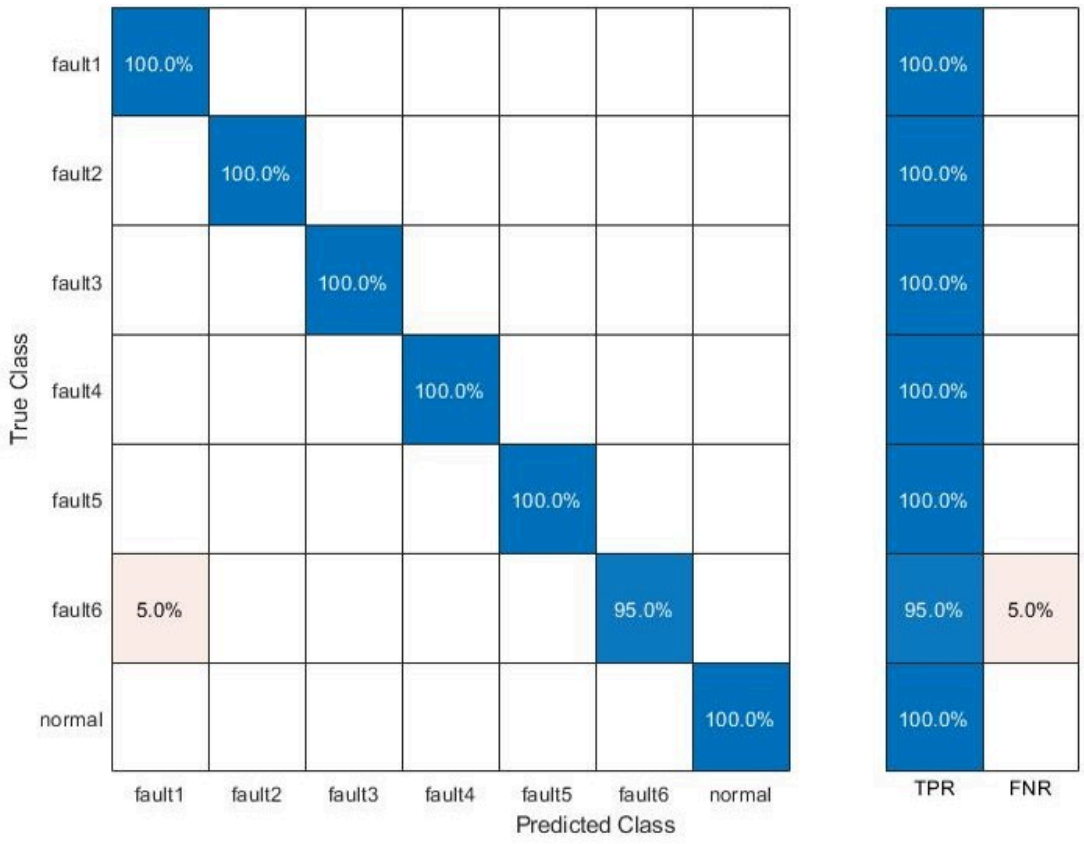

Fig. 14 The True Positive Rate (TPR) / False Negative Rate(FNR)

fault. The learning performance indices are shown in Table 6.

Mean Absolute of Errors (MAE) refers to the average values of the absolute difference between the true and predicted values in the dataset. Root Mean Square of Errors (RMSE) means the square root of the Mean Square of Errors (MSE). It measures the standard deviation of the residuals. R-Squared Score represents the ratio of the variances of the dependent variables. It is expressed as a number from 0 to 1. If the closer to 1, the better performance. For this reason, we adopt the ANN using accelerometers to diagnose the fault's degree.

D. Verification tests of fault diagnosis module

Based on the performance data of the previous section, the accelerometer data is learned using the ANN to diagnose the location and degree of damage to the actuator. Randomly damaged propellers are used to verify the performance of the proposed approach. Figure 17 shows the propeller and test environment.

About 15% of the propellers used in the verification test were damaged. 20 times tests are done at each actuator, and Figure 18 and Table 7 show the success ratio of the correct diagnosis and the average value of the degree of damage.

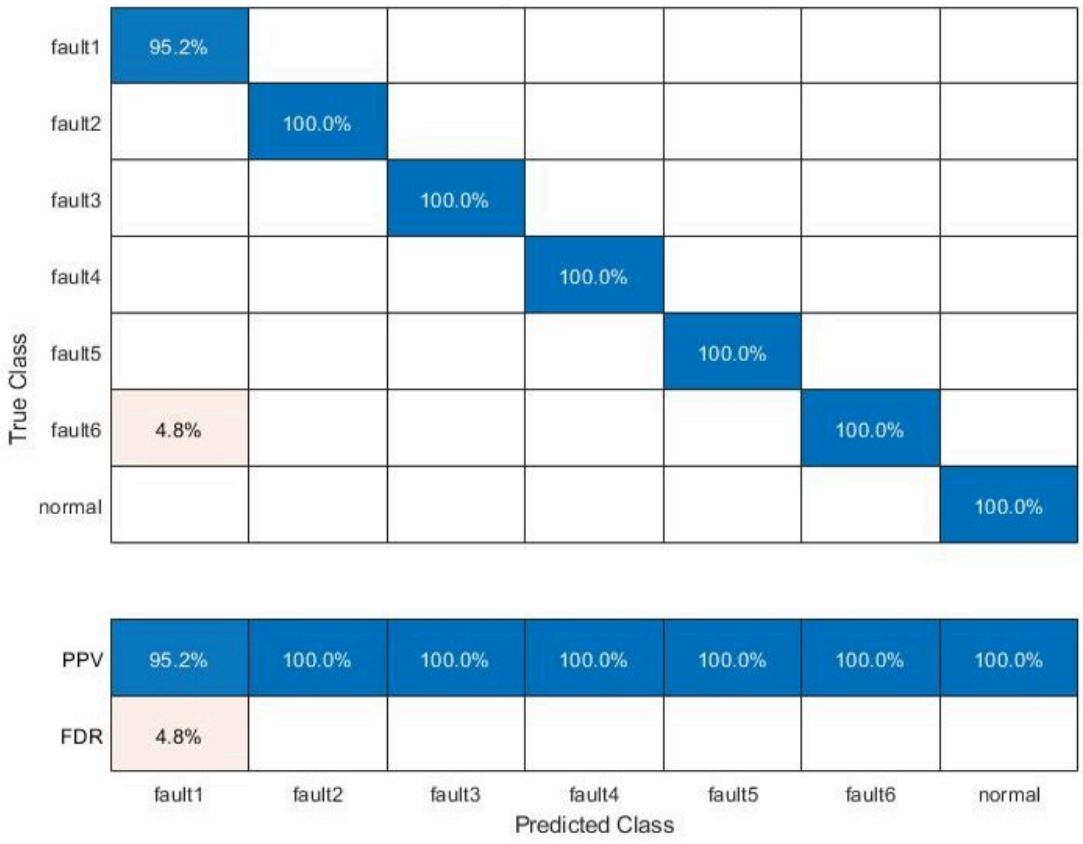

Fig. 15 The Positive Predictive Value(PPV) / False Discovery Rate(FDR)

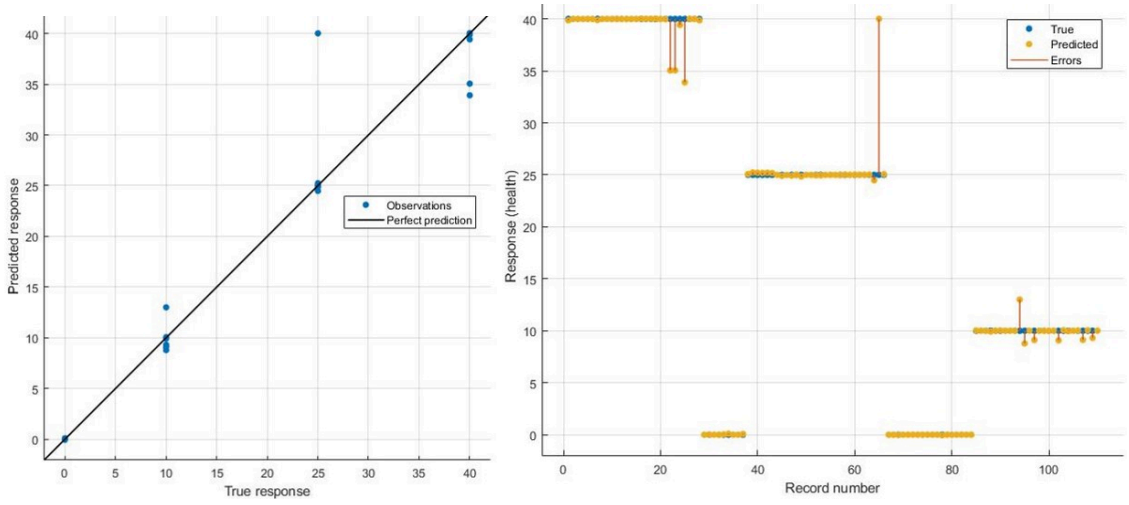

Fig. 16 Accuracy versus truth

In all cases where the experiments were conducted, the location of the thrust fault was accurately diagnosed. It was confirmed that the result was similar to the actual damage rate of 15% by diagnosing a damage rate between 11 to 17% for each actuator. These results show that fault severity diagnoses are made in nearly 10% of the training data. This

Table 5 The diagnosis result values' TPR, FNR, PPV, and FDR

Fault actuator number	TPR (%)	FNR (%)	PPV (%)	FDR (%)
Number 1 fault	100 %	0 %	95.2 %	4.8 %
Number 2 fault	100 %	0 %	100 %	0 %
Number 3 fault	100 %	0 %	100 %	0 %
Number 4 fault	100 %	0 %	100 %	0 %
Number 5 fault	100 %	0 %	100 %	0 %
Number 6 fault	95 %	5 %	100 %	0 %
Healthy	100 %	0 %	100 %	0 %
Overall performance	99.3 %	0.7 %	99.31 %	0.69 %

Table 6 Performance values of different type diagnosis method

Algorithm type	Mean absolute of errors (MAE)	Root mean square of errors (RMSE)	R-squared score
SVM (Accel)	2.5628	4.2594	0.92
ANN (Accel)	**0.41474**	**1.683**	**0.97**
SVM (Gyro)	3.0569	4.3275	0.92
ANN (Gyro)	0.5764	3.3643	0.95

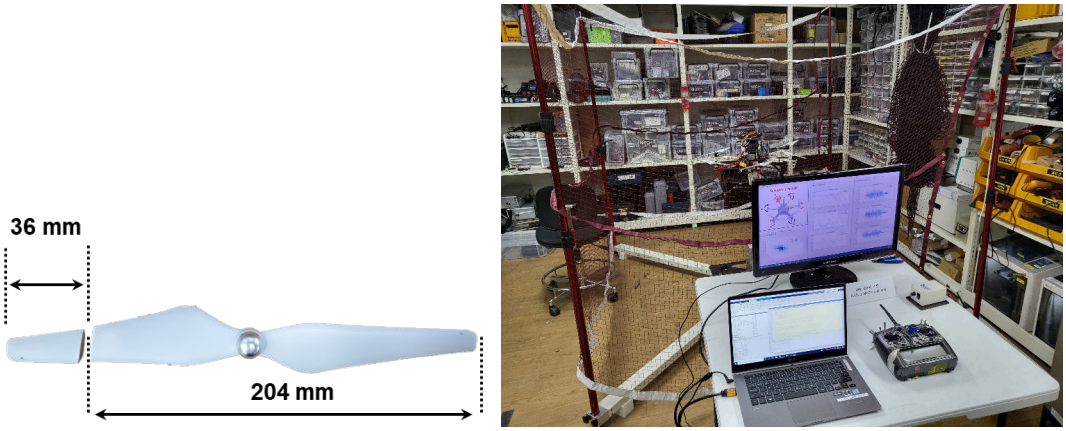

Fig. 17 The propeller and the test environment used for the verification
https://youtu.be/qL4NbXGelmQ

error is caused by the wide intervals of the data used in the regression learning process. Consequently, it is concluded that more precise diagnoses can be achieved by further subdividing the current learning data. Based on these results, if all training data intervals are subdivided, the accuracy will be higher. The test verified that the actuator's fault location and the degree of fault could be determined using only the IMU data.

V. CONCLUSION AND FUTURE WORKS

This study proposed the preflight fault diagnosis and health monitoring of hexacopter UAV actuators using the principle direction vector of the accelerometer and gyroscope dataset calculated by the PCA method. Since the

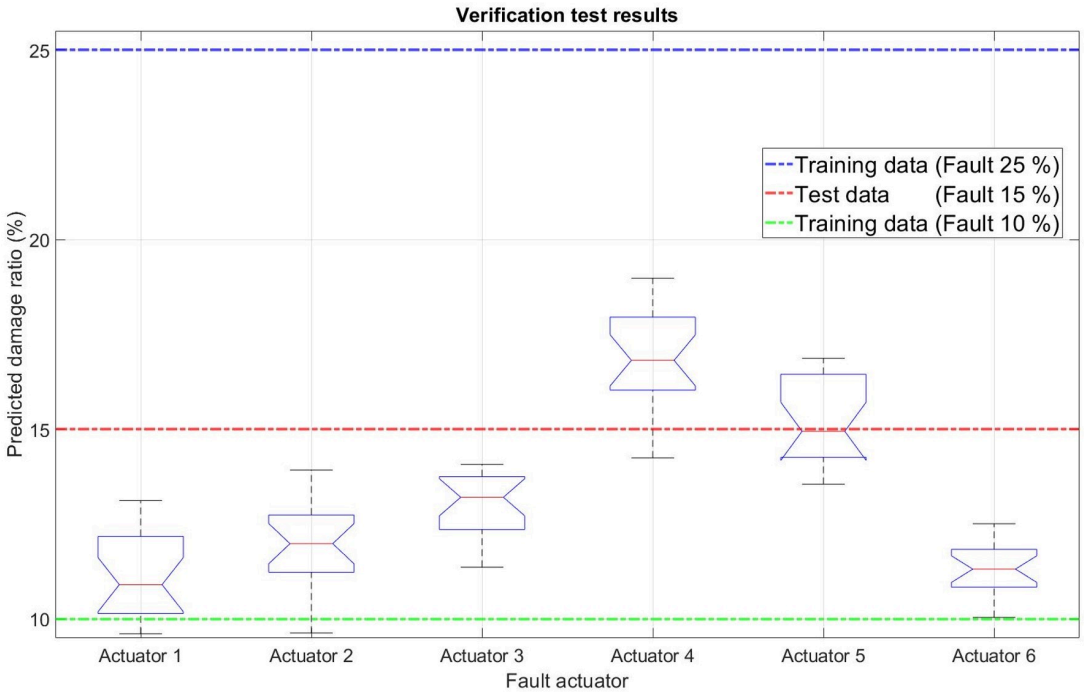

Fig. 18 Fault diagnosis results by actuator location

Table 7 The diagnosis result of verification tests

Fault actuator	Fault location diagnose success ratio	Average predicted values (%)
Actuator 1	20 / 20 (100 %)	10.914
Actuator 2	20 / 20 (100 %)	12.025
Actuator 3	20 / 20 (100 %)	13.101
Actuator 4	20 / 20 (100 %)	16.792
Actuator 5	20 / 20 (100 %)	14.964
Actuator 6	20 / 20 (100 %)	11.367

accelerometer or gyroscope datasets are collected indoors without considering wind disturbances, this FDD method is more suitable for the preflight phase before flying the hexacopter UAV in an outdoor environment. The proposed FDD method was trained to classify the thrust faults. Performance comparison was conducted according to different supervised learning algorithms. The final learning algorithm was selected by comparing the accuracy, prediction speed, and learning time. Subsequently, the reliability of the method was verified by analyzing the diagnostic and monitoring performance. As a result, the true positive rate of the FDD method was 99.3 %, the false negative rate was 0.7 %, the positive predictive value was 99.31 %, and the false discovery rate was 0.69 %. The accuracy of diagnosing the degree of damage to the actuator has a reasonably small error, so it can be used for preventive measures in preflight diagnosis. Our proposed diagnostic module consists of real sensor data, which includes inherent noise. This characteristic increases the similarity between the learning data and actual flight situations. Moreover, utilizing PCA-based data for learning enhances the robustness of the diagnosis module against noise. This approach ensures that the module can handle noisy

data and effectively extract relevant information for accurate diagnosis. In addition, accelerometers and gyroscopes can be used for fault diagnostics without adding a separate sensor thus increasing the vehicle survival rate without additional cost. This method is also applicable to any multicopter type UAV with an arbitrary number of propellers. In summary, our proposed data-driven diagnosis scheme can be easily transferable beteewn multicopter vehilces when ever their IMU data are available.

In future works, performing tests under a wider variety of environments will be necessary to verify the performance of the proposed FDD. In addition, it is planned to consider multiple-thrust faults to extend the proposed FDD. To enable real-time diagnosis under actual flight conditions, it is necessary to consider data noise. Therefore, we plan to apply moving window method that performs the diagnosis at regular intervals to process sensor data. In addition, we will improve the performance by combining with simulation-based data to compensate for the insufficient and biased data.

Acknowledgments

This research was supported by Unmanned Vehicles Core Technology Research and Development Program through the National Research Foundation of Korea(NRF) and Unmanned Vehicle Advanced Research Center(UVARC) funded by the Ministry of Science and ICT, the Republic of Korea(2020M3C1C1A01083162), the National Research Foundation of Korea(NRF) grant funded by the Korea government(MSIT)(No.2021R1A5A1031868), and (No. NRF-2021R1A2C2013363).

References

[1] Kim, T., Kim, D., Kim, S., Kim, Y., and Han, S., "Improved Optical Sensor Fusion in UAV Navigation Using Feature Point Threshold Filter," *International Journal of Aeronautical and Space Sciences*, Vol. 23, No. 1, 2022, pp. 157–168. https://doi.org/10.1007/s42405-021-00423-6.

[2] Asadi, D., Ahmadi, K., and Nabavi, S. Y., "Fault-tolerant trajectory tracking control of a quadcopter in presence of a motor fault," *International Journal of Aeronautical and Space Sciences*, Vol. 23, No. 1, 2022, pp. 129–142. https://doi.org/10.1007/s42405-021-00412-9.

[3] Zhou, Z., and Liu, Y., "A Smart Landing Platform With Data-Driven Analytic Procedures for UAV Preflight Safety Diagnosis," *IEEE Access*, Vol. 9, 2021, pp. 154876–154891. https://doi.org/10.1109/access.2021.3128866.

[4] Kim, Y., Kim, T., Kim, S., Kim, Y., and Hwang, I., "Influence Analysis of Actual Fault Cases in Unmanned Vehicle Industry and Study on Fault Tolerant Technology," *Journal of the Korean Society for Aeronautical & Space Sciences*, Vol. 50, No. 9, 2022, pp. 627–638. https://doi.org/10.5139/jksas.2022.50.9.627.

[5] Rudin, K., Ducard, G. J., and Siegwart, R. Y., "Active fault-tolerant control with imperfect fault detection information: Applications to UAVs," *IEEE Transactions on Aerospace and Electronic Systems*, Vol. 56, No. 4, 2019, pp. 2792–2805. https://doi.org/10.1109/taes.2019.2959928.

[6] Jung, W., and Bang, H., "Fault and failure tolerant model predictive control of quadrotor UAV," *International Journal of Aeronautical and Space Sciences*, Vol. 22, 2021, pp. 663–675. https://doi.org/10.1007/s42405-020-00331-1.

[7] He, Q., Zhang, W., Lu, P., and Liu, J., "Performance comparison of representative model-based fault reconstruction algorithms for aircraft sensor fault detection and diagnosis," *Aerospace Science and Technology*, Vol. 98, 2020, p. 105649. https://doi.org/10.1016/j.ast.2019.105649.

[8] Dutta, A., McKay, M., Kopsaftopoulos, F., and Gandhi, F., "Statistical residual-based time series methods for multicopter fault detection and identification," *Aerospace Science and Technology*, Vol. 112, 2021, p. 106649. https://doi.org/10.1016/j.ast.2021.106649.

[9] Kim, T., and Kim, S., "Actuator fault diagnosis and counterplan using extended kalman filter considering symmetry of hexacopter UAV," *J. Inst. Control. Robot. Syst*, Vol. 27, 2021, pp. 473–481. https://doi.org/10.5302/j.icros.2021.21.0037.

[10] Asadi, D., "Model-based fault detection and identification of a quadrotor with rotor fault," *International Journal of Aeronautical and Space Sciences*, Vol. 23, No. 5, 2022, pp. 916–928. https://doi.org/10.1007/s42405-022-00494-z.

[11] Serafini, J., Bernardini, G., Porcelli, R., and Masarati, P., "In-flight health monitoring of helicopter blades via differential analysis," *Aerospace Science and Technology*, Vol. 88, 2019, pp. 436–443. https://doi.org/10.1016/j.ast.2019.03.039.

[12] Lyu, P., Lai, J., Liu, J., Liu, H. H., and Zhang, Q., "A thrust model aided fault diagnosis method for the altitude estimation of a quadrotor," *IEEE Transactions on Aerospace and Electronic Systems*, Vol. 54, No. 2, 2017, pp. 1008–1019. https://doi.org/10.1109/taes.2017.2773262.

[13] Wang, R., Xiong, Z., Liu, J., Xu, J., and Shi, L., "Chi-square and SPRT combined fault detection for multisensor navigation," *IEEE Transactions on Aerospace and Electronic Systems*, Vol. 52, No. 3, 2016, pp. 1352–1365. https://doi.org/10.1109/taes.2016.140860.

[14] Memarzadeh, M., Matthews, B., and Templin, T., "Multiclass Anomaly Detection in Flight Data Using Semi-Supervised Explainable Deep Learning Model," *Journal of Aerospace Information Systems*, Vol. 19, No. 2, 2022, pp. 83–97. https://doi.org/10.2514/1.i010959.

[15] Shin, H., Lee, J., and Kim, P., "Causality-Seq2Seq Model for Battery Anomaly Detection," *International Journal of Aeronautical and Space Sciences*, 2022, pp. 1–10. https://doi.org/10.1007/s42405-022-00508-w.

[16] Jaramillo, J., Yildirim, E., Koru, A. T., Yucelen, T., Pakmehr, M., Dunham, J., and Lu, G., "Experimental Results on Dynamic Attitude Control Allocation for a Hexarotor Platform with Faulty Motors," *AIAA SCITECH 2022 Forum*, 2022, p. 0058. https://doi.org/10.2514/6.2022-0058.

[17] Ray, D. K., Roy, T., and Chattopadhyay, S., "Skewness scanning for diagnosis of a small inter-turn fault in quadcopter's motor based on motor current signature analysis," *IEEE Sensors Journal*, Vol. 21, No. 5, 2020, pp. 6952–6961. https://doi.org/10.1109/jsen.2020.3038786.

[18] Ghalamchi, B., Jia, Z., and Mueller, M. W., "Real-time vibration-based propeller fault diagnosis for multicopters," *IEEE/ASME Transactions on Mechatronics*, Vol. 25, No. 1, 2019, pp. 395–405. https://doi.org/10.1109/tmech.2019.2947250.

[19] Ochoa, C. A., and Atkins, E. M., "Multicopter failure diagnosis through supervised learning and statistical trajectory prediction," *2018 AIAA Information Systems-AIAA Infotech@ Aerospace*, 2018, p. 1636.

[20] Pourpanah, F., Zhang, B., Ma, R., and Hao, Q., "Anomaly detection and condition monitoring of UAV motors and propellers," *2018 IEEE SENSORS*, IEEE, 2018, pp. 1–4. https://doi.org/10.1109/icsens.2018.8589572.

[21] Chen, X., Ren, H., Bil, C., and Jiang, H.-W., "Aircraft complex system diagnosis based on design knowledge and real-Time monitoring information," *Journal of Aerospace Information Systems*, Vol. 15, No. 7, 2018, pp. 414–426. https://doi.org/10.2514/1.i010524.

[22] Ghazali, M. H. M., and Rahiman, W., "Vibration-Based Fault Detection in Drone Using Artificial Intelligence," *IEEE Sensors Journal*, Vol. 22, No. 9, 2022, pp. 8439–8448. https://doi.org/10.1109/jsen.2022.3163401.

[23] Memarzadeh, M., Matthews, B., and Templin, T., "Multiclass Anomaly Detection in Flight Data Using Semi-Supervised Explainable Deep Learning Model," *Journal of Aerospace Information Systems*, Vol. 19, No. 2, 2022, pp. 83–97. https://doi.org/10.2514/1.i010959.

[24] Kim, J., Lee, J., Kim, P., Lee, J., and Kim, S., "Preflight diagnosis of multicopter thrust abnormalities using disturbance observer and gaussian process regression," *International Journal of Control, Automation and Systems*, Vol. 19, No. 6, 2021, pp. 2195–2202. https://doi.org/10.1007/s12555-020-0164-8.

[25] Iannace, G., Ciaburro, G., and Trematerra, A., "Fault diagnosis for UAV blades using artificial neural network," *Robotics*, Vol. 8, No. 3, 2019, p. 59. https://doi.org/10.3390/robotics8030059.

[26] Ghalamchi, B., and Mueller, M., "Vibration-based propeller fault diagnosis for multicopters," *2018 International Conference on Unmanned Aircraft Systems (ICUAS)*, IEEE, 2018, pp. 1041–1047. https://doi.org/10.1109/icuas.2018.8453400.

[27] Lee, C.-H., Shin, H.-S., Tsourdos, A., and Skaf, Z., "New application of data analysis using aircraft fault record data," *Journal of Aerospace Information Systems*, Vol. 15, No. 5, 2018, pp. 297–306. https://doi.org/10.2514/1.i010577.

[28] Stevens, B. L., Lewis, F. L., and Johnson, E. N., *Aircraft control and simulation: dynamics, controls design, and autonomous systems*, John Wiley & Sons, 2015.

[29] Su, J., He, J., Cheng, P., and Chen, J., "Actuator fault diagnosis of a Hexacopter: A nonlinear analytical redundancy approach," *2017 25th Mediterranean Conference on Control and Automation (MED)*, IEEE, 2017, pp. 413–418. https://doi.org/10.1109/med.2017.7984152.

[30] Jolliffe, I. T., *Principal component analysis for special types of data*, Springer, 2002.

[31] Andrews, H., and Patterson, C., "Singular value decomposition (SVD) image coding," *IEEE transactions on Communications*, Vol. 24, No. 4, 1976, pp. 425–432. https://doi.org/10.1109/tcom.1976.1093309.

[32] Bishop, C. M., et al., *Neural networks for pattern recognition*, Oxford university press, 1995.

[33] Weston, J., Mukherjee, S., Chapelle, O., Pontil, M., Poggio, T., and Vapnik, V., "Feature selection for SVMs," *Advances in neural information processing systems*, Vol. 13, 2000.

[34] Baly, R., and Hajj, H., "Wafer classification using support vector machines," *IEEE Transactions on Semiconductor Manufacturing*, Vol. 25, No. 3, 2012, pp. 373–383. https://doi.org/10.1109/tsm.2012.2196058.

[35] Singh, L., Alam, A., Kumar, K. V., Kumar, D., Kumar, P., and Jaffery, Z. A., "Design of thermal imaging-based health condition monitoring and early fault detection technique for porcelain insulators using Machine learning," *Environmental Technology & Innovation*, Vol. 24, 2021, p. 102000. https://doi.org/10.1016/j.eti.2021.102000.

Data-driven diagnosis of multicopter thrust fault using supervised learning with inertial sensors

Kim, Taegyun

2023-09-25

Kim T, Kim S, Shin H-S. (2023) Data-driven diagnosis of multicopter thrust fault using supervised learning with inertial sensors. Journal of Aerospace Information Systems, Volume 20, Number 11, November 2023, pp. 690-701

https://doi.org/10.2514/1.I011256